The EMBO Journal Vol.17 No.6 pp.1555–1568, 1998

Proteolytic refolding of the HIV-1 capsid protein amino-terminus facilitates viral core assembly

Uta K.von Schwedler[1], Timothy L.Stemmler[1], Victor Y.Klishko[1], Su Li[1], Kurt H.Albertine[2], Darrell R.Davis[1,3] and Wesley I.Sundquist[1,4]

Departments of [1]Biochemistry, [2]Pediatrics and [3]Medicinal Chemistry, University of Utah, Salt Lake City, UT 84132, USA

[4]Corresponding author
e-mail: sundquist@medschool.med.utah.edu

After budding, the human immunodeficiency virus (HIV) must 'mature' into an infectious viral particle. Viral maturation requires proteolytic processing of the Gag polyprotein at the matrix–capsid junction, which liberates the capsid (CA) domain to condense from the spherical protein coat of the immature virus into the conical core of the mature virus. We propose that upon proteolysis, the amino-terminal end of the capsid refolds into a β-hairpin/helix structure that is stabilized by formation of a salt bridge between the processed amino-terminus (Pro1) and a highly conserved aspartate residue (Asp51). The refolded amino-terminus then creates a new CA–CA interface that is essential for assembling the condensed conical core. Consistent with this model, we found that recombinant capsid proteins with as few as four matrix residues fused to their amino-termini formed spheres *in vitro*, but that removing these residues refolded the capsid amino-terminus and redirected protein assembly from spheres to cylinders. Moreover, point mutations throughout the putative CA–CA interface blocked capsid assembly *in vitro*, core assembly *in vivo* and viral infectivity. Disruption of the conserved amino-terminal capsid salt bridge also abolished the infectivity of Moloney murine leukemia viral particles, suggesting that lenti- and oncoviruses mature via analogous pathways.

Keywords: assembly/capsid protein/human immunodeficiency virus/maturation/retrovirus

Introduction

Retroviral assembly is initially driven by polymerization of the Gag polyprotein, which forms a spherical shell associated with the inner membrane of the freshly budded particle (Figure 1). Concomitant with budding, the viral protease cleaves Gag into a series of smaller, discrete proteins. These processed proteins then rearrange to form the mature, infectious viral particle (reviewed in Kräusslich, 1996). Gag processing thereby permits the orderly transformation from a virion that is competent to assemble and bud from one cell into a virion that can disassemble and replicate in a new host cell.

The human immunodeficiency virus type 1 (HIV-1) Gag protein is proteolytically processed into the following discrete proteins and spacer peptides: matrix (MA, residues 1–132), capsid (CA, 133–363), p2 (364–376), nucleocapsid (NC, 377–432), p1 (433–448) and p6 (449–500) (Figure 1A). Upon maturation, the matrix protein remains associated with the inner viral membrane, while capsid, nucleocapsid and the viral RNA condense into the center of the virus (Figure 1B). The diploid RNA genome and associated NC proteins form an electron-dense ribonucleoprotein complex, with a concomitant increase in the thermal stability of the dimeric RNA (Fu *et al.*, 1994; Feng *et al.*, 1996). The processed capsid protein then forms a conical shell that encapsidates the RNA–NC copolymer. In the absence of Gag proteolysis, neither capsid core formation (Göttlinger *et al.*, 1989; Peng *et al.*, 1989; Schatzl *et al.*, 1991; Kaplan *et al.*, 1993; Kräusslich *et al.*, 1995) nor RNA stabilization occur (Fu *et al.*, 1994), indicating that the driving force underlying maturation is the creation of new interactions between the processed domains of Gag.

Three-dimensional structures are now available for the three major Gag-derived proteins of HIV-1, either as full-length proteins [matrix (Massiah *et al.*, 1994; Matthews *et al.*, 1994; Rao *et al.*, 1995; Hill *et al.*, 1996) and nucleocapsid (Morellet *et al.*, 1992; South and Summers, 1993)] or as a compilation of the two independent folding domains of capsid (Gamble *et al.*, 1996, 1997; Gitti *et al.*, 1996; Momany *et al.*, 1996). It is not clear, however, how accurately these proteins mimic their analogous domains within the unprocessed Gag polyprotein. Significant local structural changes may occur when Gag is cleaved, particularly given the dramatic global changes that accompany viral maturation. Indeed, the detailed structure of the processed amino-terminal domain of capsid strongly suggests that the conformation surrounding the MA–CA junction of Gag changes significantly upon proteolysis (Gamble *et al.*, 1996; Gitti *et al.*, 1996; Momany *et al.*, 1996).

The amino-terminal end of the processed capsid protein forms a β-hairpin that spans residues 1–13. The hairpin folds the charged amino-terminus of Pro1 back into the protein, where it forms a buried salt bridge with the carboxylate of Asp51 (Figures 1C and 2). Several observations suggest that the amino-terminal capsid β-hairpin forms after proteolytic cleavage at the MA–CA junction. First, the capsid amino-terminus is uncharged prior to proteolysis and thus cannot form the stabilizing salt bridge with Asp51. Moreover, the buried amino-terminus of the processed capsid protein appears sterically incompatible with a matrix protein extension or with processing by the viral protease, which recognizes the MA–CA junction in an extended conformation (Wlodawer and Erickson, 1993).

The proposed proteolytic refolding of capsid is analogous to zymogen activation in the serine proteases,

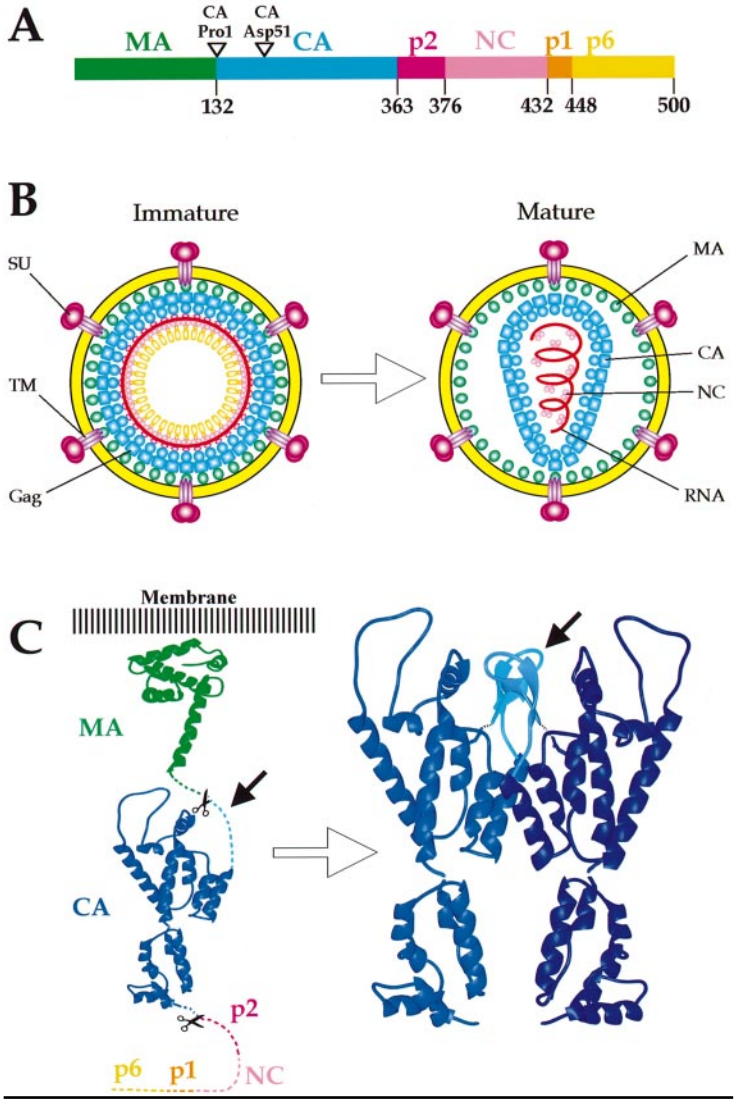

Fig. 1. Structure and maturation of the HIV-1 virion. (**A**) Domain structure of the HIV-1 Gag polyprotein. Locations of the capsid Pro1 and Asp51 residues. Color coding for the different domains of Gag is the same throughout this figure. (**B**) Schematic structures of immature and mature HIV-1 particles. The figure summarizes current models for the locations of the major virion components and emphasizes the dramatic structural rearrangements that accompany viral maturation. (**C**) Model for structural rearrangement of the HIV-1 capsid protein upon proteolytic processing at the MA–CA junction of Gag. Ribbon diagrams of the MA and CA domains of the unprocessed Gag protein (left) are based upon the crystal structures of MA (Hill *et al.*, 1996) and the amino- and carboxy-terminal domains of capsid (Gamble *et al.*, 1996, 1997). An expanded model of the processed capsid protein is shown on the right. Two molecules of capsid are shown to illustrate how folding of the capsid β-hairpin (light blue, small arrows) could be coupled to formation of a new CA–CA interface. The amino-terminal capsid interface shown is the major CA–CA interface in the co-crystal structure of CA_{151} in complex with cyclophilin A. Ribbon diagrams in Figures 1, 2 and 5 were made with the program MidasPlus (Ferrin *et al.*, 1988).

where precursor processing also causes the new amino-terminus to rearrange into a salt bridge with a buried aspartate residue (Sigler *et al.*, 1968). The energetics of the trypsinogen to trypsin folding transition have been studied in detail (Hedstrom *et al.*, 1996). In that case, the salt bridge between the amino-terminus and the buried Asp residue contributes significant stabilization energy (~3 kcal/mol), as does the packing of the amino-terminal isoleucine side chain into a hydrophobic binding site in the protein (~5 kcal/mol). Refolding of the HIV-1 capsid amino-terminus appears to be driven by a series of analogous interactions: (i) a salt bridge between the amino-terminus and Asp51, (ii) a second hydrogen bond between the amino-terminus and Gln13 O, (iii) van der Waals contacts between the invariant Pro1 ring and the C_α atoms of Ile15 and Gly46 and (iv) hydrogen bonding interactions between the two strands of the β-hairpin.

We propose that the functional consequence of capsid refolding is the creation of a new CA–CA interface in the mature capsid core (the 'amino-terminal capsid interface'). This model is depicted schematically in Figure 1C and is based upon the crystal structure of the amino-terminal domain of capsid in complex with cyclophilin A (Gamble *et al.*, 1996). The major CA–CA interface in these crystals is created by intermolecular packing of capsid helices 1 and 2 into a four-helix bundle (with their symmetry-related pairs; Figures 1C and 2). The four-helix bundle buries a total of 570 $Å^2$/subunit and exhibits a packed hydrophobic core ringed by hydrophilic interactions. Additional intermolecular interactions are formed between the

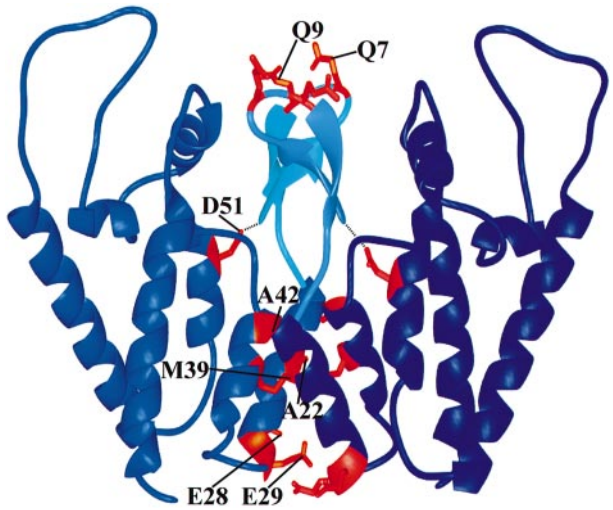

Fig. 2. Ribbon diagram of the capsid amino-terminal interface. Amino acids mutated in this study are shown in red.

two amino-terminal β-hairpins that project above the four-helix bundle (burying 230 Å^2), suggesting how folding of the capsid β-hairpin could be coupled to formation of this interface.

In summary, we propose that proteolysis at the MA–CA junction of Gag allows retroviral maturation by refolding the capsid amino-terminus and thereby facilitating the protein's rearrangement into the central conical core. Experiments described here are aimed at testing this mechanistic model for a simple developmental switch.

Results

Mutations in the capsid amino-terminal interface inhibit capsid assembly in vitro

The importance of the amino-terminal CA–CA interface for capsid assembly was tested initially using pure recombinant capsid proteins (Figure 3). *In vitro*, the HIV-1 capsid protein can assemble into long hollow cylinders (Figure 3A) which presumably utilize many of the same CA–CA interactions as the viral capsid core (Campbell and Vogt, 1995, 1997; Groß *et al.*, 1997). Although the precise relationship between the viral core and the capsid cylinders remains to be elucidated, the two structures appear to share at least a subset of similar CA–CA interactions. For example, as shown in Figure 3B, capsid cylinder assembly is blocked by a point mutation (M185A) that disrupts the well-characterized carboxy-terminal capsid dimer interface and blocks viral replication in culture (Gamble *et al.*, 1997). Instead of cylinders, CA M185A forms long strings of protein, as though destabilizing the repeating carboxy-terminal capsid dimer interface prevents the protein from winding up into a cylinder.

As described above, the amino-terminal capsid interface is composed of two distinct structural elements: the four-helix bundle and the packed β-hairpins (Figure 2). Two different capsid point mutations, M39D and D51A, were used to test the importance of each of these secondary structural elements for cylinder formation. Met39 is buried within the core of the four-helix bundle, and mutation to Asp was therefore expected to disrupt this hydrophobic core. Asp51 forms a salt bridge with the amino-terminal capsid proline residue, and mutation to Ala was expected to break the salt bridge and thereby destabilize the β-hairpin.

The wild-type and mutant capsid proteins were expressed and purified to homogeneity as described in Materials and methods. Concentrated solutions of each protein were incubated at high ionic strength for 1 h at 37°C [400 μM protein, 1 M NaCl, 50 mM Tris–HCl (pH 8.0)]. Oligomeric assemblies were collected by centrifugation, fixed and observed in thin sections by transmission electron microscopy (TEM). As shown in Figure 3A, the wild-type capsid protein efficiently assembled into hollow cylinders averaging 32 ± 2 nm in diameter (n= 20) and up to 2000 nm in length. In contrast, both amino-terminal capsid interface mutants were defective in cylinder assembly, although the two mutant proteins behaved somewhat differently.

Incubation of CA M39D under assembly conditions produced very little material that could be collected by centrifugation or discerned in thin section by TEM (Figure 3C). Oligomeric CA M39D complexes were also absent in negatively stained samples deposited directly on Formvar carbon-coated copper grids (not shown). Thus, the M39D mutation entirely abrogated the ability of capsid to form large arrays under our assembly conditions. In contrast, the CA D51A protein did form large arrays that were collected by centrifugation. However, electron micrographs revealed that the insoluble material consisted mainly of large amorphous protein aggregates. In some preparations, we observed cylinders amongst the aggregated protein (Figure 3D). Even when they formed, however, these CA D51A cylinders were shorter and far less prevalent than the wild-type CA cylinders. Thus, the D51A mutation inhibited, but did not abolish, capsid cylinder formation. Overall, the data are consistent with a role for helix 2 in cylinder formation, and suggest that the capsid β-hairpin, although not absolutely essential, also contributes to capsid assembly *in vitro*.

Matrix residues redirect capsid assembly from cylinders to spheres

The role of the MA–CA junction in capsid assembly was also examined *in vitro*, using proteins in which the final 28, 6 or 4 amino acids of matrix were fused onto the amino-terminus of CA. The first of these proteins, designated MA_{28}–CA, was designed to initiate at the first amino acid beyond the globular domain of the mature matrix protein (Massiah *et al.*, 1994; Matthews *et al.*, 1994; Hill *et al.*, 1996). The other two proteins, designated MA_6–CA and MA_4–CA, were designed to have minimal matrix extensions because NMR spectroscopic studies revealed that most (or all) of the matrix residues of MA_{28}–CA were disordered in solution (see below) and because the MA_{28}–CA protein was partially insoluble when expressed in *Escherichia coli*, presumably owing to aggregation of the disordered matrix residues.

Unlike the CA protein, the MA–CA fusion proteins did not form cylinders *in vitro*. Instead, the fusion proteins assembled into spherical particles as well as into amorphous aggregates (Figure 4). These particles were deposited on Formvar carbon-coated copper grids and visualized by negative staining (Figure 4B). The spheres formed by MA_4–CA were readily distinguishable from the CA cylinders (compare Figure 4A and B, note scale

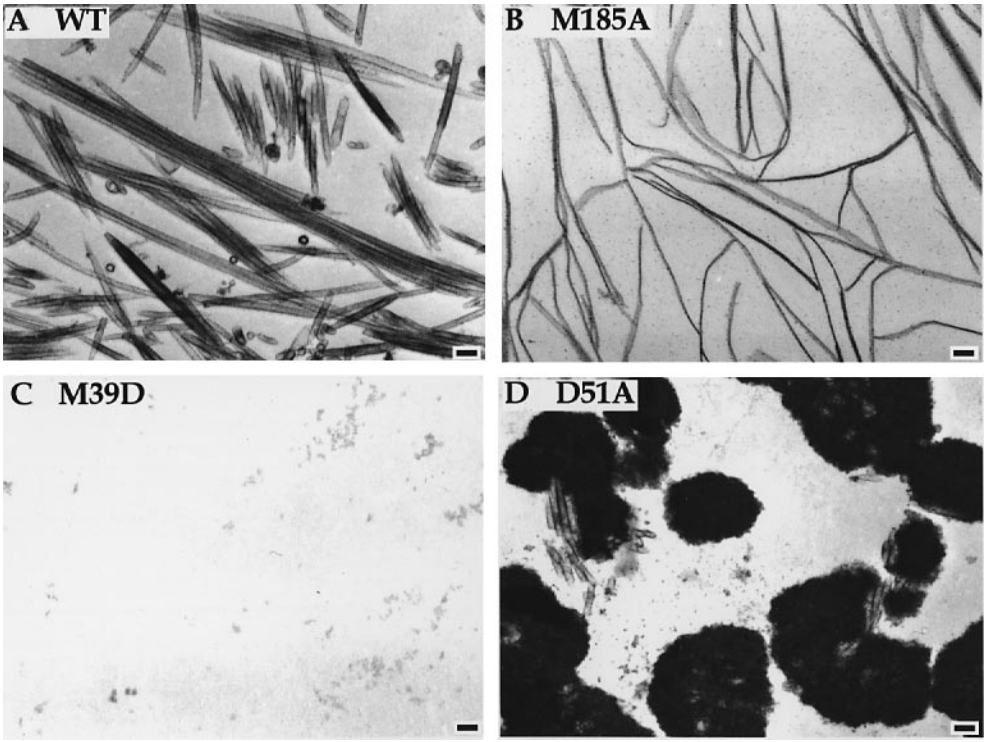

Fig. 3. Aberrant *in vitro* assembly of mutant HIV-1 capsid proteins. The figure shows representative thin-section transmission electron micrographs of the structures formed by wild-type CA (positive control) (**A**), CA M185A (negative control) (**B**), CA M39D (**C**) and CA D51A (**D**). Each protein was incubated for 1 h at 37°C in the assembly buffer (400 μM protein). Large aggregates (if any) were collected by centrifugation, fixed, stained and analyzed by thin-section TEM. The small circular structures in the micrograph of the wild-type capsid protein are hollow cylinders that were sectioned perpendicular to the cylinder axis. Note that the amorphous protein aggregates formed by CA D51A occasionally also contained imbedded cylinders. Nevertheless, the selected field shows an unusually high concentration of D51A cylinders. Cylinder widths were 32 ± 2 nm (wt CA, n=31) and 33 ± 3 nm (CA D51A, n=20). Scale bars are 100 nm.

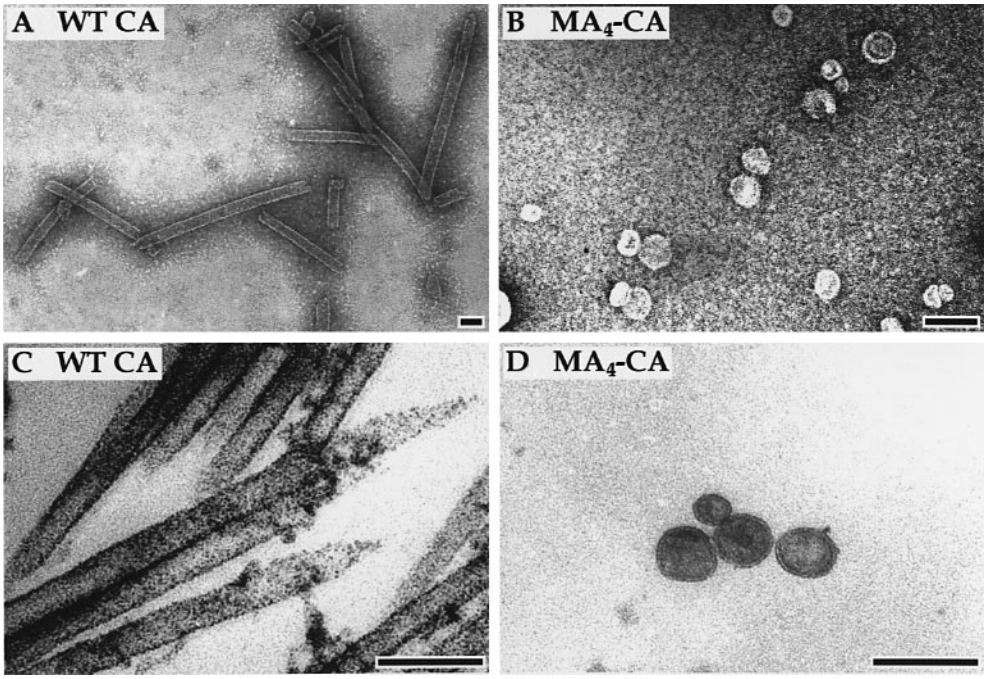

Fig. 4. Spherical assembly of the MA_4–CA protein. Left: wild-type CA (**A** and **C**), cylinders; right: MA_4–CA spheres (**B** and **D**). Direct transmission electron micrographic images of negatively stained particles are shown above (A and B), and thin-section transmission electron micrographs of positively stained particles are shown below (C and D). Particle assembly conditions are as in Figure 3. Amorphous protein aggregates were also observed in thin-section transmission electron micrographs of the MA_4–CA preparations (not shown). Scale bars are 100 nm.

changes), and in no case were cylinders observed for MA_4–CA. The MA_4–CA particles were sometimes highly spherical, but could also appear faceted and/or irregular, as has been observed for cryo-EM images of immature HIV-1 particles (Fuller *et al.*, 1997). The average diameter of the negatively stained MA_4–CA particles was 55 ± 13 nm (n=20), which is smaller than estimates for the diameter (~110 nm) of the capsid ring within the immature virion (Fuller *et al.*, 1997). The inner and outer edges of the spherical shells were often clearly defined by uranyl acetate staining of thin sections of the MA–CA fusion proteins (Figure 4D), and the thickness of the shell was 5.6 ± 0.6 nm (n=31). This thickness is compatible with models for the intact capsid protein derived from crystal structures of its composite domains, which indicate that CA spans ~60 Å in its longest dimension (Gamble *et al.*, 1997). In the three constructs tested, the efficiency of sphere formation varied inversely with the length of the matrix tail, and the MA_{28}–CA protein formed spheres very inefficiently, with most of the protein simply aggregating (data not shown).

These experiments demonstrate that fusing as few as four matrix residues onto the amino-terminus of capsid redirects protein assembly from cylinders to spheres. This transformation is strikingly reminiscent of the morphological transformation that accompanies viral maturation, where the unprocessed capsid protein initially participates in forming the spherical protein shell of the immature virus, but then rearranges into the conical core following proteolysis at the MA–CA junction.

NMR spectroscopic characterization of capsid protein constructs

NMR spectroscopy was used to test whether the protein constructs described above altered the structure of the amino-terminal end of capsid. The NMR studies were performed on monomeric proteins encompassing the first 146 or 151 residues of capsid (i.e. lacking the protein's carboxy-terminal dimerization domain). Complete proton chemical shift assignments have been reported previously for CA_{151} (Gitti *et al.*, 1996), and it was therefore possible to use amide proton NMR chemical shift perturbations as a sensitive probe for localizing structural changes in the MA_4–CA, MA_{28}–CA, CA M39D and CA D51A proteins.

The initial chemical shift analysis was performed on the MA_{28}–CA_{151} fusion protein (not shown). We identified 36 amide protons within the amino-terminal capsid domain of this protein that shifted by >0.2 p.p.m. versus the processed CA_{151} protein. The shifted residues were clustered throughout the β-hairpin and the helices against which the hairpin normally packs (1, 2, 3 and 6). As expected, all of the shifted resonances returned to their CA_{151} positions upon cleavage at the MA–CA junction with recombinant HIV-1 protease (not shown). We therefore attribute the chemical shift changes within the capsid domain to structural perturbations introduced by the additional matrix residues. Interestingly, the chemical shifts of at least 17 of the matrix residues did not change significantly upon proteolysis, indicating that the majority of matrix residues in the MA_{28}–CA_{151} protein were disordered both before and after proteolysis. Thus, this analysis suggested that the matrix residues caused refolding of the amino-terminal end of capsid, but did not themselves adopt a defined structure.

To investigate the refolding event further, we analyzed the backbone amide chemical shift changes in the shorter MA_4–CA_{146} fusion protein (capsid residues 147–151, which are disordered in CA_{151}, were deleted from this construct). The ^1H, ^{15}N heteronuclear single quantum coherence (HSQC) NMR spectra of CA_{151} (blue) and MA_4–CA_{146} (red) are shown superimposed in Figure 5A. The majority (91/134) of backbone amide proton resonances within the amino-terminal domain of capsid were not significantly shifted in the MA_4–CA protein. However, 43 amide protons were shifted by >0.2 p.p.m. in the ^1H dimension or 0.3 p.p.m. in the ^{15}N dimension upon addition of the four matrix residues. Locations of the shifted (red) and unshifted (blue) MA_4–CA_{146} residues were mapped back onto the structure of the amino-terminal domain of capsid (Figure 5B). Strikingly, the backbone amide protons of at least 26 of the first 29 capsid residues, spanning the β-hairpin and helix 1, were significantly shifted in the fusion protein. In addition, 11 of 12 residues spanning helix 3 were also significantly shifted, as were several residues in helices 2 and 6. Amide protons throughout the remainder of the protein remained unshifted (except at the very C-terminal end of the domain, presumably owing to the absence of residues 147–151), indicating that the mutation does not significantly alter the structure of helices 4, 5 and 7 (i.e. the left half of the molecule in Figure 5B). Taken together, these chemical shift analyses strongly support the model that the amino-terminal end of capsid adopts significantly different structures before and after proteolysis. We are currently determining the three-dimensional structure of the MA_4–CA fusion protein in order to define precisely how the additional matrix residues refold this region of capsid.

A similar approach was used to localize the structural changes caused by the CA M39D and D51A mutations. As shown in Figure 5C, the D51A mutation caused significant shifts in 51 of the 138 CA_{151} backbone amide protons versus the native protein. Although Asp51 is located near the amino-terminus of helix 3, chemical shift changes were again propagated throughout the β-hairpin and its adjacent helices (Figure 5D). The perturbed amide proton chemical shifts generally moved toward random coil values, indicating that disruption of the Pro1–Asp51 salt bridge altered the equilibrium to favor unfolding of the amino-terminal end of capsid. In contrast, only 19 of the 138 amide proton residues were significantly shifted in the CA M39D mutant (Figure 5E). In this case, the shifted residues clustered about the mutation site and the structural perturbations were not propagated to the amino-terminal β-hairpin (Figure 5F). This mutation therefore does not significantly disrupt the capsid structure beyond helices 1 and 2.

Point mutations within the capsid amino-terminal interface render HIV-1 non-infectious

Site-directed mutagenesis was used to examine whether the capsid amino-terminal interface is essential for viral replication. Five different point mutations designed to disrupt the interface were tested for their effects on HIV-1 replication (Figure 2). As described above, the capsid D51A mutation was designed to unfold the β-hairpin and thereby disrupt its intermolecular contacts. Capsid A22D, E28,29A,

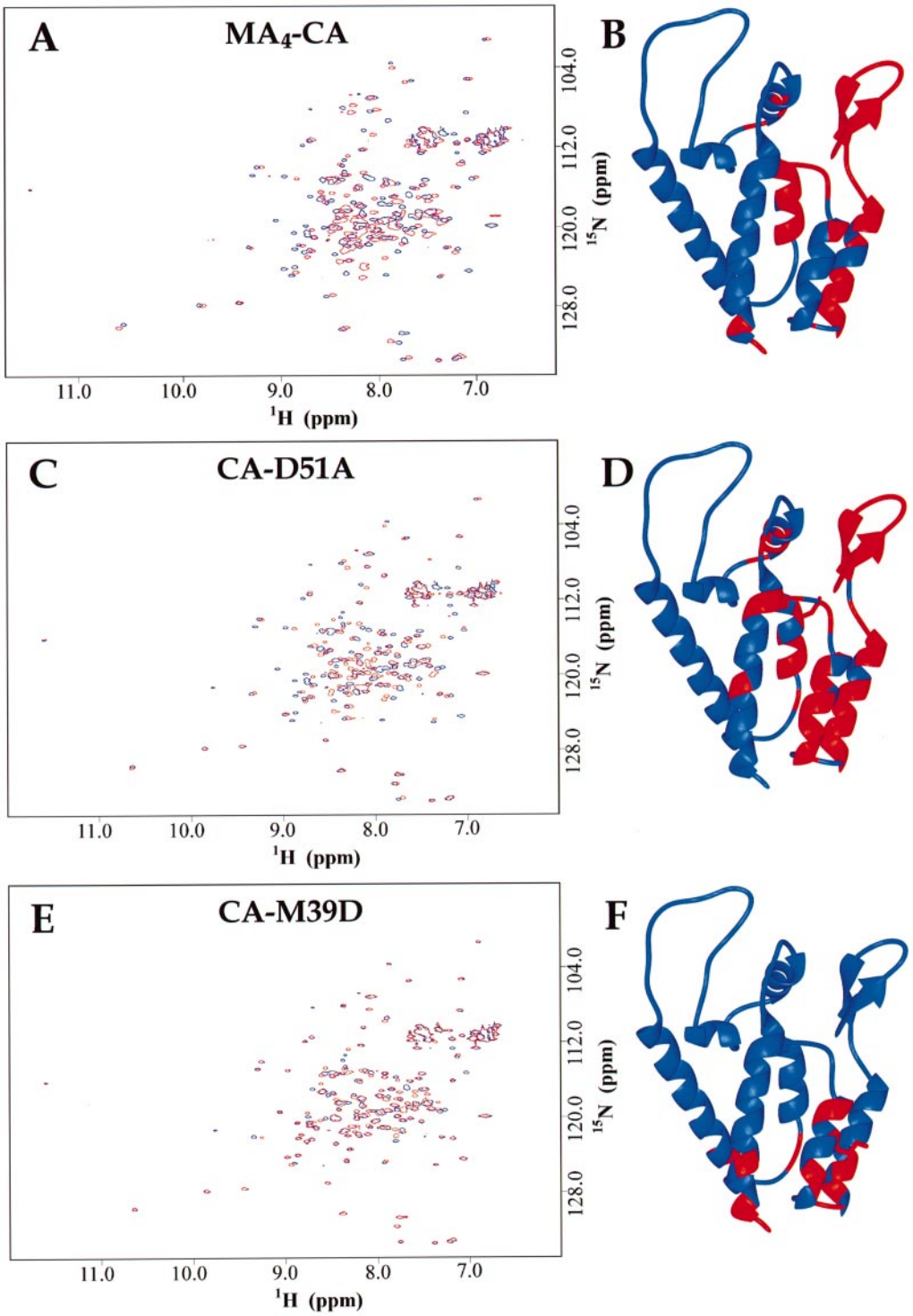

Fig. 5. NMR spectral mapping of structural perturbations in MA_4–CA_{146} (A and B), CA_{151} D51A (C and D) and CA_{151} M39D (E and F). Left: superimpositions of the ^1H,^{15}N HSQC NMR spectrum of wild-type CA_{151} (blue) upon those of MA_4–CA_{146} (**A**), CA_{151} D51A (**C**) and CA_{151} M39D (**E**) (red). Right: locations of backbone amide protons that exhibit significant chemical shift changes versus wild-type CA_{151} in MA_4–CA_{146} (**B**), CA_{151} D51A (**D**) and CA_{151} M39D (**F**). Amide protons shifted by >0.2 p.p.m. in the ^1H dimension or >0.3 p.p.m. in the ^{15}N dimension (red) are shown mapped back onto the structure of residues 1–146 of the wild-type CA_{151} protein (blue). Proline residues are depicted in the same color as their immediately adjacent residues.

M39D and A42D point mutations were designed to disrupt intermolecular packing interactions within the hydrophobic core of the four-helix bundle at the CA–CA interface. Each of the mutated residues was selected to lie on the surface of the monomeric CA protein in order to minimize intramolecular structural perturbations. A final mutation (Q7,9A) was used as a control to test the predictive power of the CA_{151} crystal structure. Gln7 and Gln9 reside on the outside of the β-hairpin loop and make no intermolecular contacts in the CA_{151} crystal structure. The Q7,9A mutation was therefore not expected to interfere significantly with capsid core assembly.

Table I. Phenotypes of HIV-1 capsid mutants

Capsid mutation	Virus production	Pelletable virus[b]	Infectivity		Cone formation
	RT/p24 assays[a]		T cell lines[c]	MAGI[d]	TEM[e]
Q7,9A	78 ± 8%	65%	4 days delayed	10%	yes
A22D	30 ± 18%	39%	no	1.6%	no
E28,29A	66 ± 10%	32%	no	0.04%	no
M39D	37 ± 17%	15%	no	0.04%	no
A42D	53 ± 8%	20%	no	0.05%	no
D51A	61 ± 45%	25%	no	0.04%	no
WT	100%	77%	yes	100%	yes

[a]Virus production from transfected 293T cells, assayed as reverse transcriptase activity and p24 CA antigen levels in the supernatant. Values from both measurements were converted to percentages of wild-type levels in each transfection, averaged, and the values are reported ± 1 SD (n=3–7). Absolute levels of wild-type virus were (19 ± 5)×10^3 c.p.m./10 μl (n=7) in RT assays and 3.5 ± 0.9 μg p24/ml (n=7) in p24 ELISA assays.
[b]Virion particles were pelleted through 20% sucrose and quantitated by p24 ELISA. The reported values are the percentage of total p24 in the supernatant that pelleted through the sucrose cushion, averaged from two experiments.
[c]Viral replication detected in SupT1, CEM and/or H9 human T cells by assaying reverse transcriptase activity in the supernatant of infected cells (growth curves).
[d]Infectivity in P4 (HeLa.CD4.LTR-β-gal) cells in a single round of infection. Blue cells per ng of p24 in the inoculum are reported as a percentage of wild-type (infectious titer 620 ± 238). Values are an average of three experiments. Note that others have also reported measurable background staining for non-infectious HIV-1 in this assay (e.g. Wu *et al.*, 1997), perhaps because Tat protein is sometimes synthesized from extrachromosomal DNA even in non-productive infections.
[e]Conical viral cores detected by TEM in thin sections of concentrated virions or of cells producing virus.

Proviral DNA constructs encoding wild-type and mutant HIV-1_{NL4-3} genomes were transfected into 293T producer cells, and viral particles were harvested from the supernatant after 2 days. Particle production was analyzed initially by assaying reverse transcriptase activity and capsid (p24) levels in the supernatant. These levels were up to 3-fold lower than wild-type for several of the mutant viruses (Table I). In order to determine the fraction of released capsid protein present in intact viral particles, the virions were purified and concentrated by centrifugation through a 20% sucrose cushion. As shown in Table I, on average 77% of the released wild-type capsid protein was pelletable, whereas this value ranged from 15 to 40% for the various mutants. Similar values were obtained for viruses produced in transfected COS-7 cells (not shown). Hence, the production of intact, stable virions was reduced 4- to 20-fold by the various amino-terminal interface mutations. Nevertheless, all of the mutants produced virions, and we therefore characterized their protein composition, infectivity and morphology.

The protein composition of the viral particles was analyzed by Western blotting of sucrose-purified virions. All of the mutant virions incorporated reverse transcriptase (Figure 6) and envelope proteins (not shown). Gag was also incorporated and processed to yield CA and MA proteins of normal size in all mutants except D51A (see below). The levels of matrix and capsid relative to the unprocessed Gag protein were generally reduced in the mutants (particularly A42D, Figure 6). These differences may reflect reduced processing of the mutant Gag proteins and/or reduced stability of the processed mutant virions during purification. Western blots of the D51A virions reproducibly showed multiple bands that corresponded to additional Gag-derived proteins, including p25, p24 and a series of truncated p24 capsid proteins. The smaller proteins presumably are degradation products that arose because the D51A mutation unfolded the protein's amino-terminus and rendered it susceptible to proteolysis.

Viral infectivity was tested initially in cultured human T cell lines. Growth curves for the wild-type and mutant

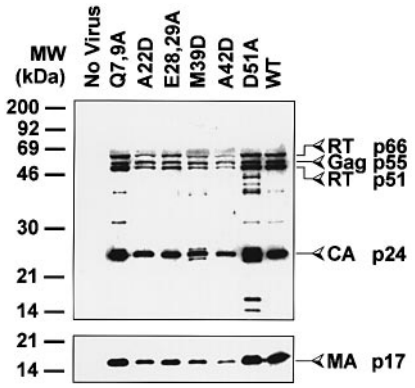

Fig. 6. Western blots of wild-type (WT) and mutant HIV-1 viruses. Virions were pelleted through sucrose and the equivalent of 100 μl of original supernatant was loaded into each lane. Primary murine antibodies against reverse transcriptase and capsid (upper panel) or rabbit anti-matrix (lower panel) were detected by enhanced chemiluminescence as described in Materials and methods. The positions of the two subunits of reverse transcriptase (p66 and p51), Gag, CA and MA proteins are shown on the right. Note that the D51A virions (and to a lesser extent, M39D virions) contain more CA–p2 (p25) and additional Gag-derived proteins, which presumably reflect non-specific proteolysis at the unfolded amino-terminus of CA.

viruses in SupT1 cells are shown in Figure 7. As expected, the wild-type virus replicated to high levels, with virus production peaking after 5–6 days and then declining as the host cells died. Replication of the Q7,9A mutant virus was delayed by 4 days versus wild-type virus, but eventually peaked at similar levels. In contrast, none of the viruses with CA amino-terminal interface mutations replicated to detectable levels at any time point tested. These mutant viruses also failed to replicate in CEM and H9 cells (data not shown). Thus, all of the mutations designed to disrupt the capsid amino-terminal interface also abolished viral replication in cultured T cells.

Viral infectivity was also tested in P4 cells in a single cycle MAGI assay (Kimpton and Emerman, 1992). As shown in Table I, every mutation designed to disrupt the capsid amino-terminal interface again dramatically

reduced viral infectivity. The titer of the A22D mutation was reduced >50-fold versus the wild-type control, and titers of the other amino-terminal interface mutants were reduced 2000-fold or more (essentially to zero, see footnote in Table I). In contrast, the Q7,9A control mutant was also reduced in infectivity, but by only 10-fold versus the wild-type virus, in good agreement with the growth curve assays.

Capsid amino-terminal interface mutants do not form conical viral cores

The mutant viral particles were examined for morphological defects using TEM (Figure 8). The most dramatic observable phenotype was the lack of conical cores in all of the amino-terminal interface mutants. At least 200 virion particles were examined for each mutant, and in no case was a conical core observed. In contrast, a significant fraction (~25%) of the mature wild-type HIV-1 and Q7,9A control virions formed discernible cores (Figure 8 A–C).

The mutant virions also exhibited apparent Gag assembly defects. Firstly, they were more difficult to concentrate and observe by TEM owing to reduced particle production. Moreover, they generally appeared more heterogeneous in size and shape than the wild-type virions. For example, size heterogeneity was evident in the electron micrographs of the CA E28,29A mutant (Figure 8E), and shape heterogeneity was evident in the micrographs of the M39D mutant (Figure 8F). Despite this heterogeneity, mutant virions with central spherical density (often acentrically located) were observed frequently, as though the RNA–NC complex had condensed, but the capsid core had failed to assemble around it (e.g. in the micrograph of the D51A mutant; Figure 8H). Immature mutant particles were also common, often with a break in the outer ring of Gag protein. Taken together, these data indicate that the amino-terminal mutations interfere with both Gag assembly and capsid maturation. These phenotypes could, of course, be causally linked. Nevertheless, the lack of cones in every one of the amino-terminal capsid interface mutants is consistent with the model that this interface plays an essential role in viral core formation.

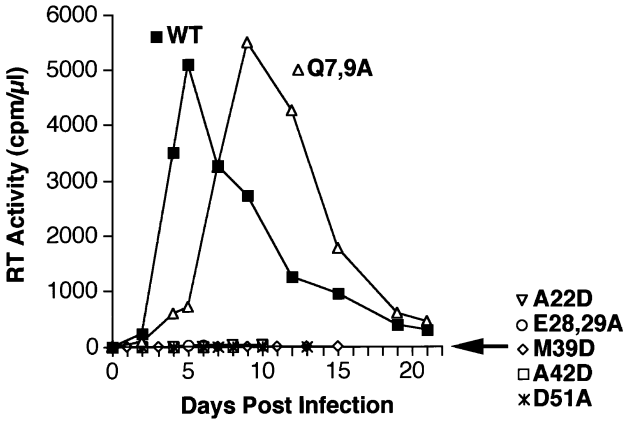

Fig. 7. Replication of wild-type (WT) and mutant HIV-1 viruses in SupT1 cells, measured as reverse transcriptase (RT) activity in the supernatant. Infections were initiated on day 0 with 10^6 reverse transcriptase c.p.m. per 10^6 cells.

Importance of the amino-terminal capsid salt bridge for MMLV replication

To evaluate the potential generality of the Pro1–Asp salt bridge, we aligned capsid protein sequences from a series

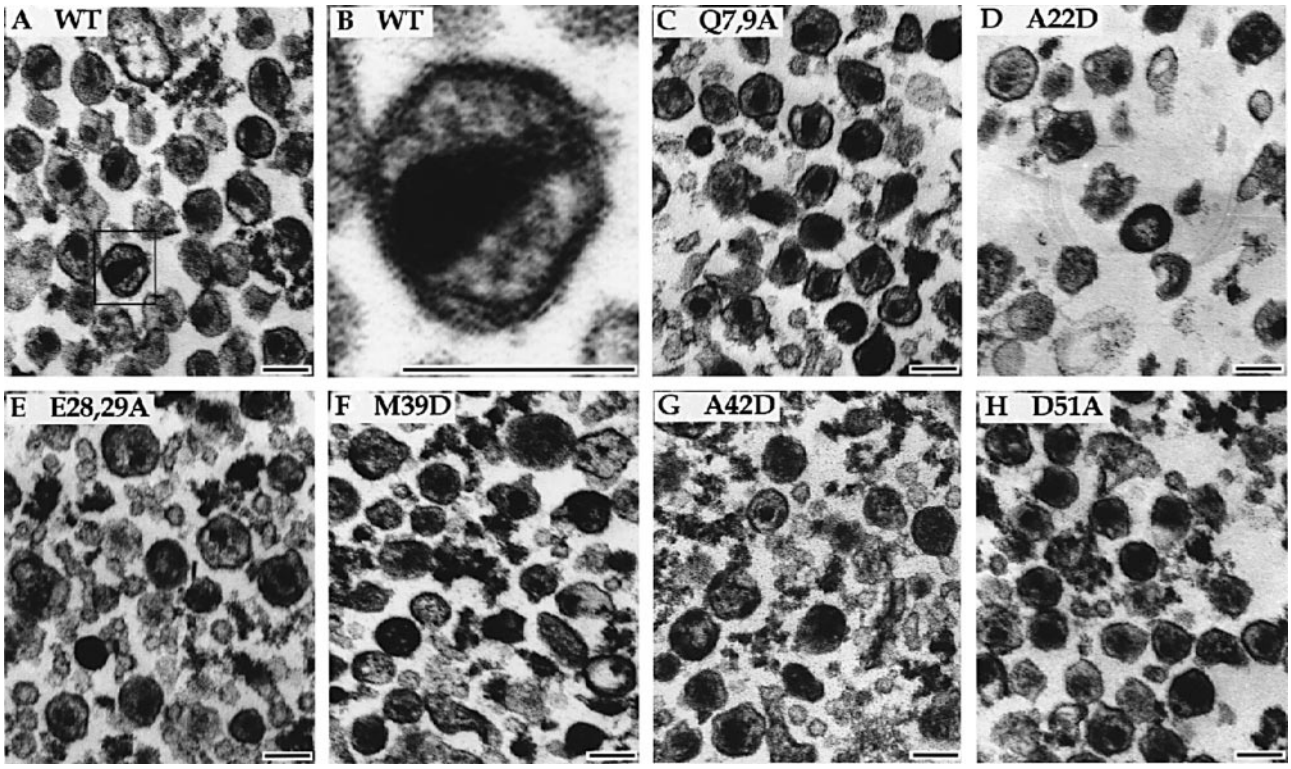

Fig. 8. Electron micrographs of wild-type (**A** and **B**) and CA mutant HIV-1 virions (**C**–**H**). The box in (A) is enlarged 5-fold in (B) to show a wild-type capsid core in detail. Note that the proportion of broken virions and/or cellular vesicles is larger in the mutant virion preparations, which have lower particle yields (Bess *et al.*, 1997; Gluschankof *et al.*, 1997). Scale bars are 100 nm in all panels.

Fig. 9. Primary sequence alignment of representative retroviral capsid proteins. The invariant Pro1 and conserved Asp (Glu) residues are highlighted by arrows. We are aware of only one exception to the invariance of Asp51 in HIV-1 strains, which is a single isolate (VI354) encoding a capsid Asn51 residue (Louwagie *et al.*, 1993). The remaining four invariant capsid residues in this alignment (shaded) are: Gly106, a residue that kinks the capsid backbone and exhibits ϕ/ψ angles (70°/22°) that are unfavorable for any other amino acid (Gamble *et al.*, 1996); and Gln155, Glu159 and Arg167, which form an interlocking hydrogen bonding network within the major homology region (MHR) (Gamble *et al.*, 1997). SIV, simian immunodeficiency virus; RSV, Rous sarcoma virus; HTLV-I, human T-cell leukemia virus type I; MMTV, mouse mammary tumor virus; JSRV, Jaagsiekte retrovirus; VISN, visna virus; FIV, feline immunodeficiency virus; BIV, bovine immunodeficiency virus; EIAV, equine infectious anemia virus; MMLV, Moloney murine leukemia virus. This alignment was created using ProPack (Feng and Doolittle, 1996).

of representative retroviruses. As shown in Figure 9, the potential to form an amino-terminal Pro1–Asp (or Glu) salt bridge is conserved across six of the seven genera of retroviruses (i.e. all but the spumaviruses) (Coffin, 1992). This conservation suggests that proteolytic refolding of capsid during maturation may occur throughout lenti- and oncoviral capsid proteins. Intriguingly, spumaviruses, which are the only retroviruses that do not undergo analogous proteolytic maturation (Gelderblom and Frank, 1987; Konvalinka *et al.*, 1995), also lack the conserved Pro and Asp residues (not shown in Figure 9).

The functional importance of the putative Pro1–Asp salt bridge was tested by mutagenesis of the C-type oncovirus Moloney murine leukemia virus (MMLV). The effect of an MMLV capsid Asp63 to Ala (D63A) mutation (equivalent to D51A in HIV-1 CA) was assayed in a single replication cycle using the MMLV pCL packaging vector system. In this system, Gag proteins from wild-type or mutant pCLeco vectors encapsidate RNA from the co-transfected retroviral vector pCLlacZ (Naviaux *et al.*, 1996). Mouse NIH-3T3 cells successfully transduced with infectious particles containing pCLlacZ produce β-galactosidase and stain blue with Xgal. However, mutations in pCLeco that impair capsid protein function will reduce the titer of the viral vector and result in fewer blue cells.

The MMLV capsid D63A mutation reduced particle release into the supernatant slightly (3- to 5-fold), as assayed by reverse transcriptase activity. Western blots of pelleted virions revealed that mutant and wild-type particles incorporated similar levels of Gag and CA, although Gag processing was slightly aberrant, with a Gag processing intermediate accumulating at higher levels in the mutant virions (Figure 10). In spite of the fact that particle production was only marginally affected, the D63A mutation again had a drastic effect on viral replication, reducing infectivity to undetectable levels (<1 infectious particle/ml), whereas the wild-type virus had titers of $(5 \pm 1)\times10^6$ infectious particles/ml. Thus, CA Asp63 is also essential for MMLV replication. Although the precise block to infectivity of this mutant was not characterized further, the major defect again arose after viral budding and is most likely improper assembly of the capsid core, indicating that similar mechanisms for capsid maturation operate in both the lentivirus HIV-1 and the oncovirus MMLV.

Discussion

Our experiments support a model in which proteolytic cleavage at the MA–CA junction of the retroviral Gag polyprotein refolds the amino-terminal end of capsid into

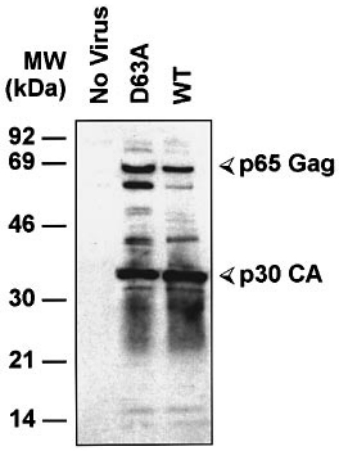

Fig. 10. Western blot of sucrose-purified MMLV particles, probed with anti-MMLV CA antiserum and detected by enhanced chemiluminescence. The positions of the Gag p65 and CA p30 proteins are shown on the right.

a β-hairpin/helix structure that is stabilized by a salt bridge between the protein's processed amino-terminus and a conserved acidic residue (Asp51 in HIV-1). The refolded capsid amino-terminus then creates a new CA–CA interface, allowing assembly of the mature capsid core. Thus, proteolysis at the MA–CA junction appears to act as a switch that redirects capsid assembly from spheres to cylinders (or cones).

Previous mutational analyses have shown that the amino-terminal domain of capsid plays an essential role in establishing viral cores of normal morphology (Dorfman *et al.*, 1994; Reicin *et al.*, 1996). Those studies revealed that core formation was abolished by deletions (Δ) or insertions (I) of multiple amino acids at capsid positions I11, Δ19–21, I20, Δ43–45 and I52. Those changes generally resulted in viral phenotypes that are similar to those reported herein (i.e. aberrant Gag assembly, heterogeneous particle production, lack of viral cores and, in some cases, defective cleavage at the CA–p2 junction). However, all of these multiple amino acid mutations fall within α-helices or β-strands, and may therefore have grossly perturbed the capsid protein structure, making it difficult to interpret the results in terms of a detailed structural model.

Guided by the crystal structure of CA_{151} (Gamble *et al.*, 1996), we designed five point mutations that were expected to disrupt the amino-terminal capsid interface, but minimize other structural perturbations. All of the mutations produced non-infectious virions that lacked conical cores. These data are consistent with, but do not prove, the hypothesis that the crystallographically defined capsid interface is also used in forming the viral core. The amino-terminal capsid interface is bipartite, consisting of packed β-hairpins (residues 1–13) and a four-helix bundle (residues 17–43). The helical interface is more extensive and more hydrophobic than the β-hairpin interface, and should therefore stabilize the CA–CA interaction to a greater extent, particularly under the high ionic strength conditions of the *in vitro* assembly assay which will favor hydrophobic interactions. Consistent with this idea, a point mutation in the helical region (M39D) completely abolished capsid cylinder formation *in vitro* whereas a mutation that destabilized the β-hairpin (D51A) merely diminished cylinder formation. Similarly, Kräusslich and co-workers have found recently that deleting the entire β-hairpin sequence blocks a recombinant capsid protein from forming cylinders in *E.coli* but not in a fully purified system (I.Groß, H.Hohenberg, C.Huckhagel and H.-G. Kräusslich, submitted).

Our amino-terminal capsid interface mutants also exhibited Gag assembly defects, which may have contributed to their reduced infectivity (as has been observed previously, e.g. Kaplan *et al.*, 1993; Pettit *et al.*, 1994; Fouchier *et al.*, 1997). Thus, our data are consistent with the hypothesis that the amino-terminal end of capsid also participates in important Gag–Gag interactions in the immature virion. The amino-terminal end of CA is clearly not the only region of Gag that is important for HIV-1 assembly, however, because even more severe viral assembly defects can be caused by mutations in other Gag domains, including MA (e.g. Kräusslich and Welker, 1996; Cannon *et al.*, 1997), the carboxy-terminal domain of CA (e.g. Dorfman *et al.*, 1994; Reicin *et al.*, 1995, 1996) and NC (e.g. Jowett *et al.*, 1992; Dorfman *et al.*, 1993). Rather, it appears that Gag makes multiple cooperative interactions along its length, allowing the Gag and Gag–Pol proteins to assemble efficiently, while excluding prematurely processed Gag proteins.

One of the most intriguing aspects of HIV-1 maturation is that Gag proteolysis switches capsid from a protein that participates in spherical particle assembly to one that assembles into a cone. Our experiments, and those of others (I.Groß, H.Hohenberg, C.Huckhagel and H.-G.Kräusslich, submitted), demonstrate that this switch can be mimicked *in vitro* simply by adding or removing as few as four matrix residues from the amino-terminus of the capsid protein. The MA residues apparently play an indirect role in controlling the capsid structure by inhibiting formation of the CA Pro1–Asp salt bridge prior to cleavage at the MA–CA junction and causing the amino-terminal end of capsid to adopt different structures before and after proteolysis. Thus, our experiments localize a key determinant of retroviral core morphogenesis to the amino-terminal end of capsid (assuming that capsid assembly *in vitro* is a valid model for HIV core morphogenesis).

We speculate that the transformation from spheres to cylinders involves converting a trimeric capsid interface to a dimeric interface. We hypothesize that HIV-1 Gag initially assembles using at least one 3-fold symmetric interaction, because the matrix protein preferentially forms trimers in the solid state (Rao *et al.*, 1995; Hill *et al.*, 1996), and because others recently have reported that the immature Gag protein forms lattices that exhibit both dimeric and trimeric interactions (Fuller *et al.*, 1997; Barklis *et al.*, 1998). In contrast, both of the crystallographically defined CA–CA interfaces of the mature capsid protein have 2-fold symmetry axes (the amino-terminal interface described herein and the carboxy-terminal dimer interface described in Gamble *et al.*, 1997). Hence, converting spheres (immature virions) to cylinders (mature virions) may involve reducing the oligomeric state of the amino-terminal capsid interface from three to two.

The apparent conservation of the putative Pro1–Asp (Glu) salt bridge suggested to us that analogous mechanisms for proteolytic refolding of capsid might be utilized across the onco- and lentiviruses. Consistent with this

model, we found that mutation of the conserved capsid Asp residue also blocked replication of the oncovirus MMLV. Campbell and Vogt (1997) have shown, however, that a MA–CA–NC fusion protein from Rous sarcoma virus (lacking the natural p10 domain between MA and CA) can assemble into cylinders *in vitro* in the presence of RNA, despite the absence of a free CA amino-terminus. This experiment may imply that different retroviruses behave differently, and/or that other regions of Gag can also play a role in determining capsid assembly properties. Indeed, dramatically different core morphologies are observed for different retroviruses (e.g. spheres, cones and cylinders), demonstrating that the detailed CA–CA interactions that determine the core morphology must differ. Nevertheless, it seems likely that the underlying organization of core assembly will be conserved, particularly given the apparent conservation of key sequences in both the amino- and carboxy-terminal domains of retroviral capsid proteins (e.g. McClure, 1991; Wills and Craven, 1991; and Figure 9). We have demonstrated recently that the cylinders formed *in vitro* by the HIV-1 capsid protein are helical (J.Finch, S.Li, V.Klishko, C.P.Hill and W.I.Sundquist, in preparation) and speculate that all viral cores will exhibit helical arrays of capsid, perhaps differing in how the helices distort to accommodate the viral RNA genome (Campbell and Vogt, 1995).

It is increasingly clear that retroviral maturation proceeds via a highly ordered pathway (Mervis *et al.*, 1988; Erickson-Viitanen *et al.*, 1989; Göttlinger *et al.*, 1989; Gowda *et al.*, 1989; Tritch *et al.*, 1991; Pettit *et al.*, 1994; Kräusslich *et al.*, 1995; Wiegers *et al.*, 1997). This is perhaps not surprising, given that the viral core assembles *de novo* at very high Gag protein concentrations (>5 mM in the virion), where non-specific aggregation may pose a significant problem. The rates of cleavage at the different HIV-1 Gag processing sites differ considerably (Mervis *et al.*, 1988; Erickson-Viitanen *et al.*, 1989; Gowda *et al.*, 1989; Kräusslich *et al.*, 1989; Pettit *et al.*, 1994), and these differences may serve to release various Gag domains as they are needed for assembly of the mature virion. Consistent with this model, viral maturation arrests at morphologically distinct stages when the different Gag processing sites are blocked (Wiegers *et al.*, 1997). The first step of viral maturation is cleavage of Gag at the p2–NC junction, which presumably liberates the NC–RNA complex to condense into the central ribonucleoprotein particle. The MA–CA junction is cleaved at an intermediate rate, releasing capsid from the membrane-bound matrix domain. Our work shows that this cleavage event also refolds the capsid amino-terminus and allows formation of a new CA–CA interface that is essential for assembling the mature capsid core. Finally, processing at the CA–p2 junction frees the capsid carboxy-terminus and allows core assembly to proceed to completion (Pettit *et al.*, 1994; Kräusslich *et al.*, 1995).

In summary, our work has defined an essential step along the HIV-1 maturation pathway. Analogous mechanisms for capsid maturation appear to be conserved across the major genera of retroviruses. This work also identifies an attractive new target of known structure for the development of novel drugs to block HIV-1 replication.

Materials and methods

Expression and purification of recombinant capsid proteins

We previously have described the cloning, mutagenesis and expression of HIV-1_{NL4-3} CA and CA_{151} from pET3a and pET11a expression vectors in BL21(DE3) cells (Studier *et al.*, 1990; Gitti *et al.*, 1996; Yoo *et al.*, 1997). Analogous mutagenesis and cloning procedures were used to introduce DNA encoding the MA–CA and mutant CA_{151} proteins into pET11a expression vectors.

Wild-type and mutant CA proteins were purified as described previously (Yoo *et al.*, 1997). The MA–CA proteins (MA_{28}–CA, MA_6–CA and MA_4–CA) were expressed and purified as follows. All steps in the purifications were performed at 4°C, and all buffers were pre-treated with 1 mM phenylmethylsulfonyl fluoride (PMSF) to minimize proteolysis. MA–CA was purified from 2 l of cultured *E.coli* 4 h after induction of protein expression with 1 μM isopropyl-β-D-thiogalactopyranoside (IPTG). Cells were harvested and resuspended in 40 ml of buffer A [25 mM Tris–HCl (pH 8.0), 5 mM β-mercaptoethanol (β-ME), 1 tablet of protease inhibitor cocktail (Boehringer Mannheim)] containing 50 mM NaCl. Cells were lysed by two passes through a French press, then sonicated to reduce viscosity. Insoluble material was removed by centrifugation at 40 000 *g* for 1 h. Crude MA–CA protein was precipitated by the addition of saturated ammonium sulfate to a final concentration of 40% (v/v), stirred on ice for 45 min and collected by centrifugation for 10 min at 3000 *g*. The pellet was redissolved in 30 ml of buffer A, dialyzed against 1 l of buffer A and chromatographed on Q Sepharose (Pharmacia) using a 400 ml linear gradient from 0 to 1 M NaCl in buffer A. The protein eluted at ~300 mM NaCl and was dialyzed overnight against buffer A containing 0.5 M ammonium sulfate. The protein was then chromatographed on phenyl Sepharose (Pharmacia) using a 200 ml linear gradient of 0.5–0 M ammonium sulfate in buffer A. The pure protein eluted during an extended wash with 0 M ammonium sulfate.

The procedure used to purify MA_{28}–CA_{151} was the same as for the full-length MA–CA proteins, with the addition of a third chromatographic purification step. Following phenyl Sepharose chromatography, the protein was dialyzed into buffer C [25 mM KMOPS (pH 6.8), 5 mM β-ME] and chromatographed on S Sepharose (Pharmacia) using a 400 ml linear gradient of 0–1 M NaCl in buffer C. Pure protein eluted at ~300 mM NaCl.

Purification of wild-type and mutant CA_{151} and MA_4–CA_{146} proteins was the same as that used for the MA–CA proteins through the first column. The proteins eluted from Q Sepharose (Pharmacia) at ~450 mM NaCl and were dialyzed overnight against 2 l of buffer D [25 mM sodium phosphate (pH 7.2), 5 mM β-ME]. The proteins were rechromatographed on Q Sepharose in buffer D and eluted with the void volume at this lower pH. The CA_{151} proteins were pure at this stage, whereas the MA_4–CA_{146} was chromatographed additionally on phenyl Sepharose (Pharmacia) using a 200 ml linear gradient of 0.5–0 M ammonium sulfate in buffer A. The pure protein eluted during an extended wash with 0 M ammonium sulfate.

Following purification, all proteins were dialyzed into the desired buffer(s) and concentrated as necessary by centrifugal filtration through a Centricon filter (Amicon). All proteins were isolated in yields of at least 10 mg/l M9 minimal medium, and their purities and identities were confirmed by SDS–PAGE, amino acid sequencing and mass spectrometry. MA_{28}–CA, MA_6–CA, MA_4–CA, MA_{28}–CA_{151} and MA_4–CA_{146} all retained non-native initiator methionine residues at their amino-termini. In contrast, all recombinant CA and CA_{151} proteins had lost their amino-terminal methionines during expression and thus corresponded exactly to the authentic CA sequence.

HIV-1 capsid protein assembly in vitro

CA cylinders and MA–CA spheres were assembled *in vitro* under the following conditions: 400 μM protein, 50 mM Tris–HCl (pH 8.0), 1 M NaCl. The mixture was incubated for 1 h at 37°C and prepared for TEM. For negatively stained TEM images, the assembled particles were adsorbed to Formvar carbon-coated copper grids by floating the grids on a drop of each sample for 30 s. The grids were rinsed with three drops of 0.1 M KCl, touched to Whatman filter paper, rinsed with three drops of saturated uranyl acetate and dried on Whatman filter paper. For thin-section TEM images, particles were collected by centrifugation in a microfuge at 13 000 r.p.m. for 1 h. Protein pellets were fixed for 12 h in 2.5% glutaraldehyde/1% paraformaldehyde in cacodylate buffer and prepared for thin-section TEM as described below for HIV-1 virions. Transmission electron micrographs were taken at magnifications of 20 000× or 80 000×.

Table II. List of primers used for generating capsid protein mutations

Oligonucleotide	Sequence	Annealing site	New restriction site
HIV-1 Q7,9A	CAGAACCTCGCGGGGGCCATGGTACATC	9–37[a]	*Sty*I
HIV-1 A22D	CTAGAACTTTAAATGACTGGGTAAAAGTAGT	50–80[a]	*Nsi*I (destroyed)
HIV-1 E28,29A	AAAGTAGTAGCAGCGAAGGCTTTC	73–96[a]	*Ear*I
HIV-1 M39D	CCAGAAGTAATACCCGATTTTAGCGCTTTATCAGAAGGAGCC	106–147[a]	*Eco*47III
HIV-1 A42D	CCCATGTTTTCAGATCTATCAGAAGGAGCC	112–141[a]	*Bgl*II
HIV-1 D51A	CCCCACAAGCGCTAAATACC	143–162[a]	*Eco*47III
MMLV D63A	GCCGTTCTCCTCTAGCGCGCTTTACAACTGG	1304–1334[b]	*Bss*HII
MMLV *Pst*I	TTCTGCTCTGCAGAATGG	732–749[b]	–
MMLV *Xho*I	GTCTGGGCGCTCGAGGGG	1574–1557[b]	–

[a]Nucleotide position in the HIV-$1_{NL4–3}$ capsid gene (with the Pro1 codon nt 1–3).
[b]Nucleotide position within MMLV plasmid p8.2B (Sitbon *et al.*, 1995).

NMR spectroscopy

NMR samples of wild-type and mutant ^{15}N-labeled CA_{151}, MA_4–CA_{146} and MA_{28}–CA_{151} proteins were 1–2 mM in 25 mM sodium phosphate buffer (pH 5.5) with 2 mM dithiothreitol (DTT) and 10% D_2O. NMR spectra were collected at 25°C on a 500 MHz Varian Unity spectrometer operating at 499.88 MHz using a Nalorac IDTG500 ^{1}H{^{15}N, ^{13}C} triple resonance probe with *z*-axis pulsed-field gradients. Two-dimensional ^{1}H, ^{15}N HSQC spectra (Bodenhausen and Ruben, 1980; Kay *et al.*, 1992; Zhang *et al.*, 1994) were collected with either WET (Smallcombe *et al.*, 1995) or WATERGATE (Piotto *et al.*, 1992) solvent suppression elements added to minimize the water signal without saturation. A total of 2048 complex data points were collected in the ^{1}H dimension and 512 increments were collected in the ^{15}N dimension. Data were transferred to a Silicon Graphics Indigo II computer, processed and analyzed using Felix 95.0 software (Biosym Technologies, San Diego). Amide proton resonances for the mutant protein were assigned by comparison with the fully resolved spectrum of the wild-type protein (Gitti *et al.*, 1996). Amide resonances were judged to be significantly shifted if they varied from the wild-type resonance by >0.2 p.p.m. in the ^{1}H dimension or >0.3 p.p.m. in the ^{15}N dimension. Amide protons in crowded regions of the spectrum were uniquely assigned to the nearest unshifted residue. The actual number of shifted residues is therefore likely to be slightly greater than reported owing to fortuitous overlap of shifted resonances.

Viral constructs

Desired point mutations were introduced into the HIV-$1_{NL4–3}$ capsid protein as follows. A 1.3 kbp *Bss*HII–*Apa*I fragment spanning the *gag* gene was subcloned from pNL4-3 into the phagemid vector pSL1180 (Pharmacia). Single-stranded DNA was isolated and used as the template for oligonucleotide-directed mutagenesis (Kunkel *et al.*, 1987). Mutant oligonucleotides introduced or eliminated restriction sites to allow facile screening (Table II), and DNA from selected clones was sequenced to confirm the mutations. *Bss*HII–*Apa*I DNA fragments containing the various mutations were then cloned back into the HIV-$1_{NL4–3}$ expression plasmid R9 (obtained as a generous gift from Dr D.Trono, Department of Genetics and Microbiology, University of Geneva Medical School) (Swingler *et al.*, 1997).

The CA D63A mutation was introduced into the MMLV packaging vector pCLeco (Naviaux *et al.*, 1996) by the 'megaprimer one tube PCR mutagenesis method' (Picard and Clark Bock, 1996). Briefly, a 254 bp 'megaprimer' was first amplified by PCR using *Pfu* polymerase (Stratagene) from pCLeco template DNA, with 10 pmol each of the MMLV-D63A upstream mutagenic primer (Table II) and the MMLV-*Xho*I downstream primer (15 cycles). Fifty pmol of the upstream MMLV-*Pst*I primer were then added to amplify an 830 bp fragment, using the previously synthesized 'megaprimer' fragment as the downstream primer (15 cycles). The 830 bp PCR fragment was digested with *Pst*I and *Xho*I, gel-purified, cloned back into the partially *Pst*I-/completely *Xho*I-digested vector pCLeco, and the D63A mutation was confirmed by direct DNA sequencing.

HIV-1 production and infectivity

Wild-type and mutant HIV-$1_{NL4–3}$ R9 plasmids were transiently transfected into 293T human embryonic kidney cells carrying the SV40 large T antigen (Pear *et al.*, 1993) as previously described (Naviaux *et al.*, 1996). Supernatants were harvested after 32–44 h, and virus production quantitated in p24 enzyme-linked immunosorbent assay (ELISA) (Dupont) and reverse transcriptase assay (Goff *et al.*, 1981). Viral infectivity was assayed by infecting 10^6 SupT1, CEM or H9 human T cells with mutant and wild-type viruses at levels equivalent to 1×10^6 c.p.m. of reverse transcriptase activity or 100 ng of p24. Cells were grown in RPMI with 10% fetal calf serum, glutamine and penicillin/streptomycin. Supernatant samples were collected from the infected cultures every 1–3 days, and cells were split 1:2 or 1:3 afterwards as necessary. SupT1 and CEM cells were obtained from the NIH AIDS Research and Reference Reagent Program, and H9 cells were obtained from Dr D.Trono.

Viral infectivity in a single-round infection assay (MAGI assay) was quantitated in P4 HeLa.CD4.LTR-β-gal cells (Charneau *et al.*, 1994) as described previously (Kimpton and Emerman, 1992). P4 cells carry the β-galactosidase gene under the control of the HIV-1 long terminal repeat which is activated by Tat protein synthesized from the infecting virus. Thus, infected cells express β-galactosidase and stain blue with Xgal. Infected cells were counted after 48 h, with infectivity reported as the number of blue cells per ng of p24 of input virus.

MMLV replication assays

The effect of the capsid D63A mutation on MMLV replication was assayed in a single replication cycle using the pCL packaging vector system (Naviaux *et al.*, 1996). Infectious titers in NIH 3T3 cells (from Dr Mark Meuth, University of Utah) were determined by transducing 4×10^4 cells overnight with serial dilutions of the retroviral vector in the presence of 8 μg/ml polybrene, and fixing and staining the cells with Xgal 48 h later (Naviaux *et al.*, 1996). Wild-type titers of undiluted supernatants were 5×10^6 and 6×10^6 infectious particles/ml in two independent experiments. The MMLV pCLeco packaging system was obtained as a generous gift from Dr R.Naviaux, UCSD, San Diego and Dr I.Verma, Salk Institute, La Jolla.

Western blotting

Virus from the supernatants of transfected cells was pelleted through a 20% sucrose cushion in a microcentrifuge for 90 min at 13 000 r.p.m. and resuspended in 25 μl of SDS gel loading buffer. Samples (2 μl) were separated by 12% PAGE, transferred, blocked, blotted with antisera, and protein bands were detected by enhanced chemiluminescence (DuPont) as described (von Schwedler *et al.*, 1993). Primary antibodies used were: a murine anti-reverse transcriptase monoclonal antibody at 1:500 [obtained from Dr Stephen Hughes through the NIH AIDS Research and Reference Reagent Program, cat. #3483 (Ferris *et al.*, 1990)], monoclonal antibody CA76C against HIV-1 CA [NIH AIDS Research and Reference Reagent Program, cat. #383 (Steimer *et al.*, 1986)], a rabbit anti-HIV-1 MA at 1:50 000 (from Dr D.Trono), a sheep anti-HIV Env at 1:5000 [obtained from Dr Mark Page and Dr Robin Thorp through the NIH AIDS Research and Reference Reagent Program, cat. # 567 (Page *et al.*, 1991)] and a goat anti-MMLV p30 at 1:2000 (obtained from Dr John Elder, Scripps Institute, La Jolla). Horseradish peroxidase-conjugated secondary antibodies were as follows: anti-rabbit at 1:4000 (Amersham), anti-mouse at 1:1000 (Cappel), anti-sheep at 1:5000 (Cappel) and anti-goat at 1:4000 (Jackson ImmunoResearch).

Transmission electron microscopy

The virus-containing supernatants of transfected cells were adjusted to 20% fetal calf serum and 2.5% glutaraldehyde in cacodylate buffer [0.1 M sodium cacodylate (pH 7.4), 35 mM sucrose, 4 mM $CaCl_2$] and centrifuged in a microfuge at 13 000 r.p.m. for 90 min at 4°C. The supernatants were aspirated, and the pellets were fixed further in 100 μl of 2.5% glutaraldehyde in cacodylate buffer at 4°C overnight. The pellets were washed thoroughly with buffer, post-fixed for 60 min with 2%

OsO_4 in buffer, rinsed with buffer and water, stained *en bloc* for 30 min with a saturated aqueous solution of uranyl acetate (~3%, pH 4), dehydrated in a graded acetone series and embedded in epoxy resin EMbed-812 (Electron Microscopy Sciences). Thin sections (60–90 nm) were picked up on copper grids, stained for 20 min on drops of saturated uranyl acetate, rinsed with water, touched to Whatman filter paper, then stained for 10 min on drops of Reynolds' lead citrate in the presence of NaOH pellets (Reynolds, 1963), rinsed with water and dried on Whatman paper. Electron micrographs were taken on a Hitachi H-7100 transmission electron microscope at an accelerating voltage of 75 kV and a magnification of 50 000×.

Acknowledgements

We thank Chris Hill, Theresa Gamble and Sanghee Yoo for helpful discussions on the structural basis for capsid assembly; Maureen McMurray, Hui Wang and Nancy Chandler for technical assistance; and Eric Barklis and Hans-Georg Kräusslich for preprints of their work. We also thank Hans-Georg Kräusslich for sharing his experimental results on the assembly of MA–CA fusion proteins prior to publication. This work was supported by NIH grants RO1 AI40333, RO1 AI37524 (to W.I.S.) and S10 RR10489 (to K.H.A.).

References

Barklis,E., McDermott,J., Wilkens,S., Fuller,S. and Thompson,D. (1998) Organization of HIV-1 capsid proteins on a lipid monolayer. *J. Biol. Chem.*, **273**, in press.

Bess,J.W.J., Gorelick,R.J., Bosche,W.J., Henderson,L.E. and Arthur,L.O. (1997) Microvesicles are a source of contaminating cellular proteins found in purified HIV-1 preparations. *Virology*, **230**, 134–144.

Bodenhausen,G. and Ruben,D.J. (1980) Natural abundance nitrogen-15 NMR by enhanced heteronuclear spectroscopy. *Chem. Phys. Lett.*, **69**, 185–189.

Campbell,S. and Vogt,V.M. (1995) Self-assembly *in vitro* of purified CA–NC proteins from Rous sarcoma virus and human immunodeficiency virus type 1. *J. Virol.*, **69**, 6487–6497.

Campbell,S. and Vogt,V.M. (1997) *In vitro* assembly of virus-like particles with Rous sarcoma virus Gag deletion mutants: identification of the p10 domain as a morphological determinant in the formation of spherical particles. *J. Virol.*, **71**, 4425–4435.

Cannon,P.M., Matthews,S., Clark,N., Byles,E.D., Iourin,O., Hockley, D.J., Kingsman,S.M. and Kingsman,A.J. (1997) Structure/function studies of the human immunodeficiency type 1 matrix protein, p17. *J. Virol.*, **71**, 3474–3483.

Charneau,P., Mirambeau,G., Roux,P., Paulous,S., Buc,H. and Clavel,F. (1994) HIV-1 reverse transcription: a termination step at the center of the virus. *J. Mol. Biol.*, **241**, 651–662.

Coffin,J. (1992) Structure and classification of retroviruses. In Levy,J.A. (ed.), *The Retroviridae.* Plenum Press, New York, pp. 19–49.

Dorfman,T., Luban,J., Goff,S.P., Haseltine,W.A. and Göttlinger,H.G. (1993) Mapping of functionally important residues of a cysteine–histidine box in the human immunodeficiency virus type 1 nucleocapsid protein. *J. Virol.*, **67**, 6159–6169.

Dorfman,T., Bukovsky,A., Öhagen,Å., Höglund,S. and Göttlinger,H.G. (1994) Functional domains of the capsid protein of human immunodeficiency virus type 1. *J. Virol.*, **68**, 8180–8187.

Erickson-Viitanen,S., Manfreidi,J., Viitanen,P., Tribe,D.E., Tritch,R., Huttchinson,C.A.I., Loeb,D.D. and Swanstrom,R. (1989) Cleavage of HIV-1 Gag polyprotein synthesized *in vitro*: sequential cleavage by the viral protease. *AIDS Res. Hum. Retro.*, **5**, 577–591.

Feng,D.-F. and Doolittle,R.F. (1996) Progressive alignment of amino acid sequences and construction of phylogenetic trees from them. *Methods Enzymol.*, **266**, 368–382.

Feng,Y.-X., Copeland,T.D., Henderson,L.E., Gorelick,R.J., Bosche,W.J., Levin,J.G. and Rein,A. (1996) HIV-1 nucleocapsid protein induces 'maturation' of dimeric retroviral RNA *in vitro*. *Proc. Natl Acad. Sci. USA*, **93**, 7577–7581.

Ferrin,T.E., Huang,C.C., Jarvis,L.E. and Langridge,R.J. (1988) The Midas display system. *Mol. Graphics*, **6**, 13–27.

Ferris,A.L., Hizi,A., Showalter,S., Pichuantes,S., Babe,L., Craik,C.S. and Hughes,S.H. (1990) Immunological and proteolytic analysis of HIV-1 reverse transcriptase structure. *Virology*, **175**, 456–464.

Fouchier,R.A.M., Meyer,B.E., Simon,J.H.M., Fischer,U. and Malim, M.H. (1997) HIV-1 infection of non-dividing cells: evidence that the amino-terminal basic region is important for Gag processing but not for post-entry nuclear import. *EMBO J.*, **16**, 4531–4539.

Fu,W., Gorelick,R.J. and Rein,A. (1994) Characterization of human immunodeficiency virus type 1 dimeric RNA from wild-type and protease-defective virions. *J. Virol.*, **68**, 5013–5018.

Fuller,S.D., Wilk,T., Bowen,B.E., Kräusslich,H.-G. and Vogt,V.M. (1997) Cryo-electron microscopy reveals ordered domains in the immature HIV-1 particle. *Curr. Biol.*, **7**, 729–738.

Gamble,T., Vajdos,F., Yoo,S., Worthylake,D., Houseweart,M., Sundquist,W.I. and Hill,C.P. (1996) Crystal structure of human cyclophilin A bound to the amino-terminal domain of HIV-1 capsid. *Cell*, **87**, 1285–1294.

Gamble,T., Yoo,S., Vajdos,F., Worthylake,D., Wang,H., Sundquist,W. I. and Hill,C.P. (1997) Structure of the carboxyl-terminal dimerization domain of the HIV-1 capsid protein. *Science*, **278**, 849–853.

Gelderblom,H. and Frank,H. (1987) Spumavirinae. In Nermut,M.V. and Steven,A.C. (eds), *Animal Virus Structure.* Elsevier Science Publishers, Amsterdam, pp. 305–311.

Gitti,R.K., Lee,B.M., Walker,J., Summers,M.F., Yoo,S. and Sundquist,W.I. (1996) Structure of the amino-terminal core domain of the HIV-1 capsid protein. *Science*, **273**, 231–235.

Gluschankof,P., Mondor,I., Gelderblom,H.R. and Sattentau,Q.J. (1997) Cell membrane vesicles are a major contaminant of gradient-enriched human immunodeficiency virus type-1 preparations. *Virology*, **230**, 125–133.

Goff,S.P., Traktman,P. and Baltimore,D. (1981) Isolation and properties of Moloney murine leukemia virus mutants: use of a rapid assay of release of virion reverse transcriptase. *J. Virol.*, **38**, 239–248.

Göttlinger,H.G., Sodroski,J.G. and Haseltine,W.A. (1989) Role of capsid precursor processing and myristoylation in morphogenesis and infectivity of human immunodeficiency virus type 1. *Proc. Natl Acad. Sci. USA*, **86**, 5781–5785.

Gowda,S.D., Stein,B.S. and Engleman,E.G. (1989) Identification of protein intermediates in the processing of the p55 HIV-1 gag precursor in cells infected with recombinant vaccinia virus. *J. Biol. Chem.*, **264**, 8459–8462.

Groß,I., Hohenberg,H. and Kräusslich,H.-G. (1997) *In vitro* assembly properties of purified bacterially expressed capsid proteins of human immunodeficiency virus. *Eur. J. Biochem.*, **249**, 592–600.

Hedstrom,L., Lin,T.-Y. and Fast,W. (1996) Hydrophobic interactions control zymogen activation in the trypsin family of serine proteases. *Biochemistry*, **35**, 4515–4523.

Hill,C.P., Worthylake,D., Bancroft,D.P., Christensen,A.M. and Sundquist,W.I. (1996) Crystal structure of the HIV-1 matrix protein: implications for viral architecture and assembly. *Proc. Natl Acad. Sci. USA*, **93**, 3099–3104.

Jowett,J., Hockley,D., Nermut,M.V. and Jones,I.M. (1992) Distinct signals in human immunodeficiency virus type 1 Pr55 necessary for RNA binding and particle formation. *J. Gen. Virol.*, **73**, 3079–3086.

Kaplan,A.H., Zack,J.A., Knigge,M., Paul,D.A., Kempf,D.J., Norbeck, D.W. and Swanstrom,R. (1993) Partial inhibition of the human immunodeficiency virus type 1 protease results in aberrant virus assembly and the formation of non-infectious particles. *J. Virol.*, **67**, 4050–4055.

Kay,L.E., Keifer,P. and Saarinen,T. (1992) Pure absorption gradient enhanced heteronuclear single quantum correlation spectroscopy with improved sensitivity. *J. Am. Chem. Soc.*, **114**, 10663–10665.

Kimpton,J. and Emerman,M. (1992) Detection of replication-competent and pseudotyped HIV with a sensitive cell line on the basis of activation of an integrated β-galactosidase gene. *J. Virol.*, **66**, 2232–2239.

Konvalinka,J., Loechelt,M., Zentgraf,H., Fluegel,R.M. and Kräusslich, H.-G. (1995) Active foamy virus proteinase is required for virus infectivity but not for formation of a Pol polyprotein. *J. Virol.*, **69**, 7264–7268.

Kräusslich,H.-G. (1996) *Morphogenesis and Maturation of Retroviruses.* Current Topics in Immunology. Springer-Verlag, Berlin.

Kräusslich,H.-G. and Welker,R. (1996) Intracellular transport of retroviral capsid components. In Kräusslich,H.-G. (ed.), *Morphogenesis and Maturation of Retroviruses.* Current Topics in Immunology. Springer-Verlag, Berlin, pp. 25–63.

Kräusslich,H.-G., Ingraham,R.H., Skoog,M.T., Wimmer,E., Pallai,P.V. and Carter,C.A. (1989) Activity of purified biosynthetic proteinase of human immunodeficiency virus on natural substrates and synthetic peptides. *Proc. Natl Acad. Sci. USA*, **86**, 807–811.

Kräusslich,H.-G., Fäcke,M., Heuser,A.M., Konvalinka,J. and Zentgraf,H. (1995) The spacer peptide between human immunodeficiency virus capsid and nucleocapsid proteins is essential for ordered assembly and viral infectivity. *J. Virol.*, **69**, 3407–3419.

Kunkel,T.A., Roberts,J.D. and Zakour,R.A. (1987) Rapid and efficient site-specific mutagenesis without phenotypic selection. *Methods Enzymol.*, **154**, 367–382.

Louwagie,J. *et al*. (1993) Phylogenetic analysis of gag genes from 70 international HIV-1 isolates provides evidence for multiple genotypes. *AIDS*, **7**, 769–780.

Massiah,M., Starich,M.R., Paschall,C.M., Summers,M.F., Christensen, A.M. and Sundquist,W.I. (1994) Three dimensional structure of the human immunodeficiency virus type 1 matrix protein. *J. Mol. Biol.*, **244**, 198–223.

Matthews,S. *et al*. (1994) Structural similarity between the p17 matrix protein of HIV-1 and interferon-γ. *Nature*, **370**, 666–668.

McClure,M.A. (1991) Evolution of retroposons by acquisition or deletion of retrovirus-like genes. *Mol. Biol. Evol.*, **8**, 835–856.

Mervis,R.J., Ahmad,N., Lillehoj,E.P., Raum,M.G., Salazar,R.F.H., Chan,H.W. and Venkatesan,S. (1988) The *gag* gene products of human immunodeficiency virus type 1: alignment with the *gag* open reading frame, identification of posttranslational modifications, and evidence for alternative *gag* precursors. *J. Virol.*, **62**, 3993–4002.

Momany,C. *et al*. (1996) Crystal structure of dimeric HIV-1 capsid protein. *Nature Struct. Biol.*, **3**, 763–770.

Morellet,N., Jullian,N., De Rocquigny,H., Maigret,B., Darlix,J.-L. and Roques,B.P. (1992) Determination of the structure of the nucleocapsid protein NCp7 from the human immunodeficiency virus type 1 by ^{1}H NMR. *EMBO J.*, **11**, 3059–3065.

Naviaux,R.K., Costanzi,E., Haas,M. and Verma,I.M. (1996) The pCL vector system: rapid production of helper-free, high-titer, recombinant retroviruses. *J. Virol.*, **70**, 5701–5705.

Page,M., Mills,K.H.G., Schild,G.C., Ling,C., McKnight,A., Barnard, A.L., Dilger,P. and Thorpe,R. (1991) Studies on the immunogenicity of Chinese hamster ovary cell-derived recombinant gp120 (HIV-1_{IIIB}). *Vaccine*, **9**, 47–52.

Pear,W.S., Nolan,G.P., Scott,M.L. and Baltimore,D. (1993) Production of high-titre helper-free retroviruses by transient transfection. *Proc. Natl Acad. Sci. USA*, **90**, 8392–8396.

Peng,C., Ho,B.K., Chang,T.W. and Chang,N.T. (1989) Role of human immunodeficiency virus type 1-specific protease in core protein maturation and viral infectivity. *J. Virol.*, **63**, 2550–2556.

Pettit,S.C., Moody,M.D., Wehbie,R.S., Kaplan,A.H., Natermet,P.V., Klein,C.A. and Swanstrom,R. (1994) The p2 domain of human immunodeficiency virus type 1 Gag regulates sequential proteolytic processing and is required to produce fully infectious virions. *J. Virol.*, **68**, 8017–8027.

Picard,V. and Clark Bock,S. (1996) PCR cloning protocols. In White,B. (ed.), *Methods in Molecular Biology.* Humana Press, Totowa, NJ, pp. 183–188.

Piotto,M., Saudek,V. and Sklenár,V. (1992) Gradient-tailored excitation for single-quantum NMR spectroscopy of aqueous solutions. *J. Biomol. NMR*, **2**, 661–665.

Rao,Z., Belyaev,A.S., Fry,E., Roy,P., Jones,I.M. and Stuart,D.I. (1995) Crystal structure of SIV matrix antigen and implications for virus assembly. *Nature*, **378**, 743–747.

Reicin,A.S., Paik,S., Berkowitz,R.D., Luban,J., Lowy,I. and Goff,S.P. (1995) Linker insertion mutations in the human immunodeficiency virus type 1 *gag* gene: effects on virion particle assembly, release, and infectivity. *J. Virol.*, **69**, 642–650.

Reicin,A.S., Ohagen,A., Yin,L., Hoglund,S. and Goff,S.P. (1996) The role of Gag in human immunodeficiency virus type 1 virion morphogenesis and early steps of the viral life cycle. *J. Virol.*, **70**, 8645–8652.

Reynolds,E.S. (1963) Use of lead citrate at high pH as an electron-opaque stain in electron microscopy. *J. Cell. Biol.*, **17**, 208–212.

Schatzl,H., Gelderblom,H.R., Nitschko,H. and von der Helm,K. (1991) Analysis of non-infectious HIV particles produced in presence of HIV proteinase inhibitor. *Arch. Virol.*, **120**, 71–81.

Sigler,P.B., Blow,D.M., Mathews,B.W. and Henderson,R. (1968) Structure of crystalline α-chymotrypsin II. A preliminary report including a hypothesis for the activation mechanism. *J. Mol. Biol.*, **35**, 143–164.

Sitbon,M., Ellerbrok,H., Pozo,F., Nishio,J., Hayes,S.F., Evans,L.H. and Chesebro,B. (1995) Sequences in the U5-*gag-pol* region influence early and late pathogenic effects of Friend and Moloney murine leukemia virus. *J. Virol.*, **64**, 2135–2140.

Smallcombe,S.H., Patt,S.L. and Keifer,P.A. (1995) WET solvent suppression and its applications to LC NMR and high resolution NMR spectroscopy. *J. Magn. Resonance*, **117**, 295–303.

South,T.L. and Summers,M.F. (1993) Zinc- and sequence-dependent binding to nucleic acids by the N-terminal zinc finger domain of the HIV-1 nucleocapsid protein: structure of the complex with the psi-site analogue, d(ACGCC). *Protein Sci.*, **2**, 3–19.

Steimer,K.S. *et al*. (1986) Differential antibody responses of individuals infected with AIDS-associated retroviruses surveyed using the viral core antigen p25 *gag* expressed in bacteria. *Virology*, **150**, 283–290.

Studier,F.W., Rosenberg,A.H., Dunn,J.J. and Dubendorff,J.W. (1990) Use of T7 RNA polymerase to direct expression of cloned genes. *Methods Enzymol.*, **185**, 60–89.

Swingler,S., Gallay,P., Camaur,D., Song,J., Abo,A. and Trono,D. (1997) The Nef protein of human immunodeficiency virus type 1 enhances serine phosphorylation of the viral matrix. *J. Virol.*, **71**, 4372–4377.

Tritch,R.J., Cheng,Y.-S., Yin,F.H. and Erickson-Viitanen,S. (1991) Mutagenesis of protease cleavage sites in the human immunodeficiency virus type 1 *gag* polyprotein. *J. Virol.*, **65**, 922–930.

von Schwedler,U., Song,J., Aiken,C. and Trono,D. (1993) Vif is crucial for human immunodeficiency virus type I proviral synthesis in infected cells. *J. Virol.*, **67**, 4945–4955.

Wiegers,K., Rutter,G., Kottler,H., Tessmer,U., Hohenberg,H. and Kräusslich,H.-G. (1997) Sequential steps in HIV particle maturation revealed by mutations of individual Gag polyprotein cleavage sites. *J. Virol.*, **72**, in press.

Wills,J. and Craven,R. (1991) Form, function, and use of retroviral Gag proteins. *AIDS*, **5**, 639–654.

Wlodawer,A. and Erickson,J.W. (1993) Structure-based inhibitors of HIV-1 protease. *Annu. Rev. Biochem.*, **62**, 543–585.

Wu,X., Liu,H., Xiao,H., Conway,J.A., Hunter,E. and Kappes,J.C. (1997) Functional RT and IN incorporated into HIV-1 particles independently of the Gag/Pol precursor protein. *EMBO J.*, **16**, 5113–5122.

Yoo,S., Myszka,D., Yeh,C.-y., McMurray,M., Hill,C.P. and Sundquist,W.I. (1997) Molecular recognition in the HIV-1 capsid/cyclophilin A complex. *J. Mol. Biol.*, **269**, 780–795.

Zhang,O., Kay,L.E., Olivier,J.P. and Forman-Kay,J.D. (1994) Backbone ^{1}H and ^{15}N resonance assignments of the N-terminal SH3 domain of Drk in folded and unfolded states using enhanced-sensitivity pulsed field gradient NMR techniques. *J. Biomol. NMR*, **4**, 845–858.

Received November 14, 1997; revised and accepted January 19, 1998